Time-Resolved Fluorescence and Solvatochromy of Directly Linked Pyrene−DMA Derivatives in Alcoholic Solution

Simone Techert,[*,†] **Alexander Wiessner,**[†] **Stefan Schmatz,**[‡] **and Hubert Staerk**[*,†]

Max-Planck-Institut für biophysikalische Chemie, Abteilung Spektroskopie und Photochemische Kinetik, Am Fassberg 11, D-37077 Göttingen, Germany, and Institut für Physikalische Chemie der Universität Göttingen, Tammannstrasse 6, D-37077 Göttingen, Germany

Picosecond transient absorption spectroscopy and picosecond spectro-streak fluorescence measurements have been carried out in order to understand the complex photophysical dynamics of directly linked donor−acceptor systems and the solvation dynamics in longer-chain alcohols. With these techniques, the fast solvent response to optically generated charge transfer (CT) species can be followed. Studies were performed on covalently linked donor−acceptor systems of the type pyrene with derivatives of *N,N*-dimethylaniline: dimethyl-(4-pyren-1-yl-phenyl)-amine, dimethyl-(3-methyl-4-pyren-1-yl-phenyl)-amine and (3,5-dimethyl-4-pyren-1-yl-phenyl)-dimethylamine. The results are interpreted with particular emphasis on solvation dependent electronic restructuring of the CT species. We suggest a mechanism where the adiabatic electronic restructuring coincides with the coupling to the torsional degrees of freedom of the solvent.

I. Introduction

Electron transfer (ET) reactions are fundamental processes in chemistry and biology. Recently, pyrene derivatives as partners in electron donor−acceptor systems have been introduced as fluorescence probes in biophysical chemistry. Unlike other aromatic compounds, pyrenes have turned out to be unique candidates for such studies. The fluorescence intensity and lifetime of pyrene can change significantly upon hybridization of a covalently linked oligonucleotide to a DNA/RNA-target strand and these characteristics are used for sequence-specific detection of nucleic acids in solution.[1] These biological applications are of high interest: directly linked donor acceptor systems are subject to strong electronic couplings. However, these systems with pyrene as an electron acceptor are characterized by a high fluorescence quantum yield, allowing for applications such as a distributed feedback charge-transfer dye laser in the liquid or solid state, as well as other applications in the field of photonic devices.[2−4] In this context, bipyridine-substituted pyrene derivatives are also of high scientific interest since they connect the unique spectroscopic features of pyrene with the unique properties of Ru(bpy)$_3^{2+}$ complexes, leading to systems with new photophysical reaction pathways, e.g., reversible triplet−triplet energy transfer.[4,5]

In this work, we report on the dynamical spectroscopic response of the three directly linked electron donor−acceptor systems of the pyrene type with derivatives of *N,N*-dimethyl-aniline (DMA) in solution. Chemically, the systems differ only in the methyl substitution on the DMA moiety (see Figure 1). The systems studied are dimethyl-(4-pyren-1-yl-phenyl)-amine (**PyDMA**), dimethyl-(3-methyl-4-pyren-1-yl-phenyl)-amine (**PyMDMA**), and (3,5-dimethyl-4-pyren-1-yl-phenyl)-dimethyl-amine (**PyDMDMA**).

The different DMA derivatives act as electron donor, and the pyrene moiety as electron acceptor. The positive inductive
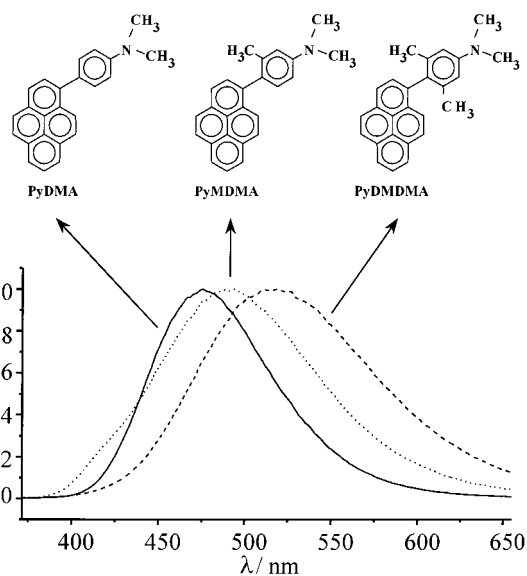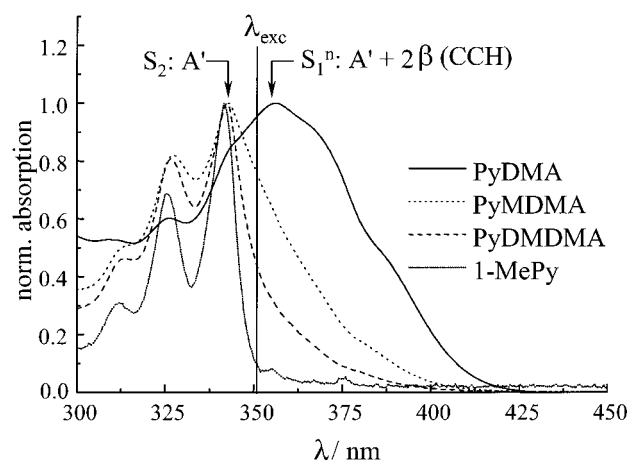

Figure 1. Normalized stationary emission spectra of PyDMA, PyMDMA, and PyDMDMA in hexanol.

effect of the methyl moieties on the electron donor changes the redox properties of the system, and this influences the CT characteristics. From previous experiments on free systems it is known that every additional methyl group on the phenyl ring leads to a decrease of the oxidation potential by approximately 0.08 eV.[6]

Due to the lack of an extended bridge between the electron donor and acceptor moieties in the systems presented in this work, the physical characteristics of these groups themselves strongly influence the ET mechanism. Recently, picosecond time-resolved X-ray diffraction studies on electronically highly coupled systems with phenyl-DMA moieties have shown that, at least in a molecular crystal, the large amplitude motions of the DMA moiety (inversion and torsion) influence the relaxation

---

[†] Max-Planck-Institut für Biophysikalische Chemie
[‡] Institut für Physikalische Chemie der Universität Göttingen.

Figure 2. Normalized stationary absorption spectra of PyDMA, PyMDMA, and PyDMDMA in hexanol compared to 1-methylpyrene in hexanol.

pathway on the potential energy surface (PES) of the excited electronic state.[7,8] However, in conjunction with pyrene,[3,9,10] which is well known for its typical vibronic couplings of the first and second electronically excited state,[11-13] additional effects are found for PyDMA that differ from the physical response of phenanthrene-DMA or anthracene-DMA, where phenanthrene or anthracene acts as an electron acceptor.[14,15] In the case of 9-anthracene-DMA (AnDMA),[2,16,17,18] e.g., where the DMA moiety is substituted at position 9 of anthracene, the experimental stationary and time-resolved results are rationalized by superposition of two different conformers: Calculations suggest that these conformers can be distinguished mainly by the dihedral angle between the phenyl moiety and the $N(CH_3)_2$ group. According to the absorption spectra, one of these conformers is thought to be formed through a π π^* transition and the other conformer through direct absorption into a CT state with high ionic character. Exciting in the blue shifted π π^* band (the locally excited state (LE)) causes the system to undergo a solvent-dependent adiabatic fast relaxation into the intramolecular charge transfer (ICT) state.[16,17]

In contrast, PyDMA, PyMDMA, and PyDMDMA in solution show only one fluorescing emission band (Figure 1), though also here two emission bands, one originating from a locally excited state and one occurring from an ICT state, should be expected. The increased Stokes shift in the emission spectra (see Figure 1) also reflects the decreasing electronic coupling between pyrene and DMA with the number of substituents on the DMA moiety.

Since in the bisubstituted compound PyDMDMA the donor and acceptor groups are twisted 90° against each other, PyDMDMA is electronically the most decoupled of all ICT systems studied in this work and exhibits an absorption spectrum most similar to that of 1-methylpyrene (Figure 2). UV absorption and emission spectroscopy and photon counting measurements published recently[3] also show that in PyDMA,[2,9,10,19] PyMDMA, and PyDMDMA the first excited electronic state has pronounced CT character.

To understand whether, in addition to the unusual one-band emission behavior, geometrical changes as postulated in An-DMA play an important role in the CT generation and relaxation of PyDMA, PyMDMA, and PyDMDMA, in this work we concentrate on a detailed experimental characterization of the species that causes this one-band emission by applying the complementary techniques of transient fluorescence emission (spectro-streak) and transient absorption spectroscopy. Further-

more, we will present a more detailed study of the interaction between CT generation and the retarded response of protic solvents, elucidating the complexity of electronic effects and geometrical changes of solute and solvent. Longer chain alcohols are chosen as solvents, since the extended carbon chains provide low-frequency, large amplitude torsional modes that might interact with the large amplitude motions (torsion and inversion) of PyDMA to PyDMDMA.

This paper is organized as follows. The experimental setups are briefly reviewed in section II. In section III the results are reported and discussed. Section IV contains our conclusions.

II. Experimental Section

A. Synthesis and Sample Preparation. Synthesis and sample characterization of the three compounds have been described earlier.[3] The solutions used in the experiment were degassed employing the freeze−pump−thaw method. The concentrations of the sample solutions were in the order of 10^{-5} M. To exclude saturation effects, the concentrations of the solution were optimized for the excitation wavelength of interest (351−355 nm), so that the optical density (oD) at 355 nm was 0.5−1.0 in a 1-cm thick cuvette.

B. Methods and Apparatus. The early experimental strategy was to determine the parameters of the solvation process globally in order to separate them from the actual fluorescence intensity decay. Otherwise, recording of the fluorescence decays at a fixed wavelength and in the presence of a (in the present case bathochromic) band shift due to solvation dynamics, the kinetic parameters could not be disentangled. To overcome difficulties in measurements of a series of time functions at a certain number of different wavelengths and their calibrated composition to a global histogram, which include nontrivial data treatment and normalization strategies, the spectro-streak technique was developed.[20,21] With this technique, time- and wavelength-resolved transient fluorescence signals can be studied.

The time-resolved CT fluorescence spectra discussed in section III were observed using this spectro-streak technique. A detailed description of the setup of this new type of photometer is contained in the references.[20,21] A special feature of the design is the three-dimensional detection, where the intensity of the fluorescence band can be measured simultaneously in one shot as a function of time and wavelength. The spectro-streak apparatus consists of a home-constructed grating objective (4−15 ps time resolution, depending on the apperture used) attached to a streak camera (Hamamatsu C1370−01, 2 ps time-resolution) with a CCD camera as detector unit. The samples were excited with the third harmonic (351 nm) of a mode-locked Nd:glass laser. The pulse width of this laser was about 7 ps. The whole measuring unit (the tandem: grating objective, streak camera, image intensifier and CCD camera) was positioned perpendicular to the propagation direction of the excitation beam. To exclude orientational relaxation effects, the polarization direction of the excitation light was adjusted to the magic angle of 54.74°.

The transient absorption spectra were recorded using a pump−probe spectrometer with 45 ps time resolution. A detailed description of the pump−probe setup can be found in references 22 and 23. The third harmonic (355 nm) of a mode-locked Nd: YAG laser was used as pump source with a pulse width of 25 ps to 30 ps. As the probe light, a white light continuum was used which was generated via nonlinear mixing of the 1064 nm fundamental pulse in a mixture of H_2O/D_2O. Each transient absorption measurement was corrected for the spontaneous fluorescence light, which was measured with blocked back-

Directly Linked Donor−Acceptor System Dynamics

J. Phys. Chem. B, Vol. 105, No. 31, 2001 **7581**
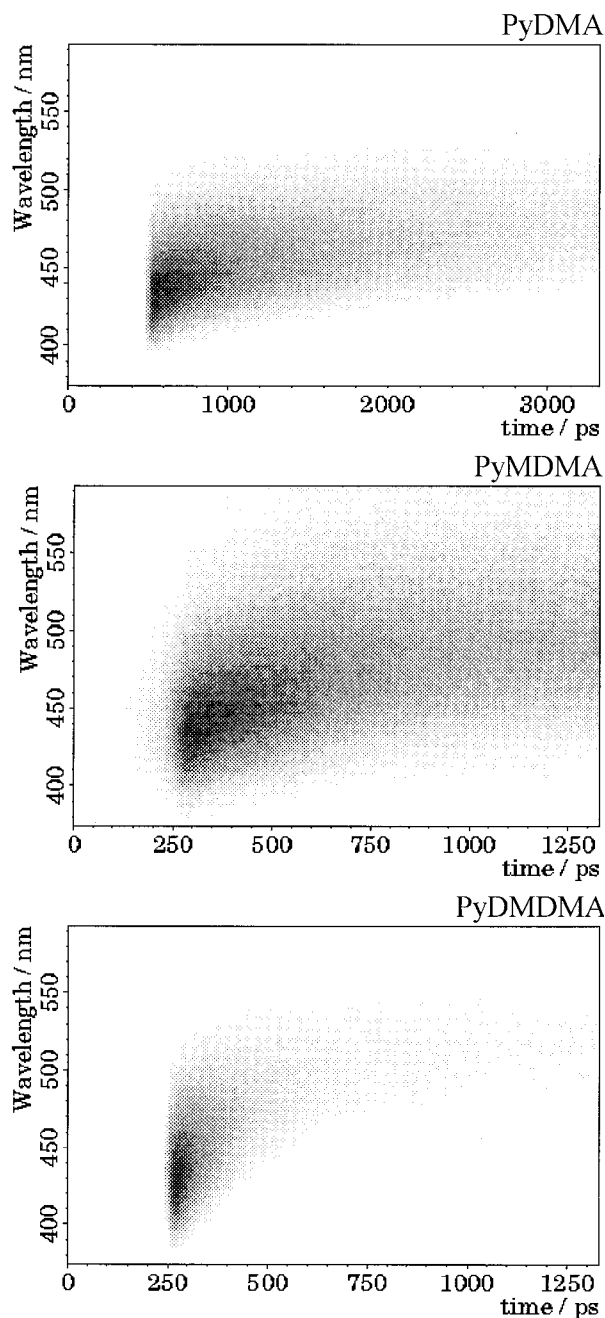
Figure 3. Spectro-streak snapshots of the time-resolved CT fluorescence emission of PyDMA (top), PyMDMA (middle), and PyDMDMA (bottom) in hexanol.

ground light. For the measurement of the transient spectra of possibly generated triplet species, a commercial Xenon flashlamp with 50 μs time resolution was used as pump source in the transient absorption setup.

III. Results and Discussion

Transient Fluorescence Emission Experiments. Figure 3 shows the three-dimensional spectro-streak snapshots of PyDMA (top), PyMDMA (middle), and PyDMDMA (bottom) in hexanol. The time-resolved differences in the behavior of PyDMA, PyMDMA, and PyDMDMA are obvious even before binning and integrating the raw data. The response function of the solvent, after the CT species was generated, is detected and characterized as a smearing of the fluorescence intensity with respect to time along the wavelength scale toward longer

wavelengths, yielding intensity/wavelength/time information. For all three shots, the same intensity scaling was used. Employing appropriate binning modes, provided by the two-dimensional CCD camera, leads to time evolutions of the emission spectra as shown in Figure 4 (PyDMA, left; PyMDMA, middle; and PyDMDMA, right). The spectra shown in Figure 4 are the raw data that are not $n^3\tilde{\nu}^3$ corrected. The $n^3\tilde{\nu}^3$ correction is generally necessary if one is interested in relative population data, since the emission of the dipole is proportional to $\tilde{\nu}^3$. In none of the spectra could an emission band originating from a locally excited state be found. Whereas the spectro-streak measurements of PyMDMA are comparable to the results of PyDMA, in PyDMDMA the fast (about 200 ps) Stokes shift is associated with a fast intensity decrease on the same time scale, followed by a nanosecond decay.

The spectro-streak measurements reveal two characteristic dependences: first, they show the time evolution of the maximum of the emission band (the solvatochromic effect, yielding the solvation time τ_s), and second they allow the evaluation of the time evolution of the intensity of the band by integrating the fitted and extrapolated band over the entire wavelength range. The time dependence of the bathochromic fluorescence shift is determined as follows: After applying the $n^3 \tilde{\nu}^3$ correction, the total emission bands were fitted to a log-normal function, yielding $\tilde{\nu}_{max}$.[24] The fit also enables to extrapolate the emission band beyond the measurement range (instrumental cutoff wavelength). Thus, the time-dependent Stokes shift can be described by the correlation function

$$C(t) = \frac{\tilde{\nu}_{max}(t) - \tilde{\nu}_{max}(\infty)}{\tilde{\nu}_{max}(0) - \tilde{\nu}_{max}(\infty)} \tag{1}$$

and the solvation time τ_s. Here, $\tilde{\nu}_{max}(\infty)$ is the maximum of the CT band at long times and is taken from the stationary fluorescence measurement.

Table 1 summarizes the characteristics of the solvation dynamics for PyDMA, PyMDMA, and PyDMDMA in hexanol and octanol at different temperatures. In the case of PyDMA in octOH, double exponential fits were found to be satisfactory. In this case, the mean times $\langle \tau_s \rangle$ of multiexponential fits according to

$$\langle \tau_s \rangle = \sum_{i=1}^{n} A_i \tau_i \bigg/ \sum_{i=1}^{n} A_i \tag{2}$$

were used, where the amplitudes A_i (in cm^{-1}) and the lifetimes τ_i are fit parameters. The τ_i are obtained from the exponential decay components $A_i \exp(-t/\tau_i)$. For the calculation of the longitudinal relaxation times τ_L and τ_{LD}, two models were used. Model 1 is based on the Debye continuum model where the solvent is treated as a structureless, noninteracting dielectric continuum. In this case, the solvent can be characterized by just one Debye dispersion region expressed in a monoexponential relaxation behavior and leading to the relaxation time[25,26]

$$\tau_L = \frac{\epsilon_\infty}{\epsilon} \tau_D \tag{3}$$

where ϵ is the static dielectric constant and τ_D denotes the Debye relaxation time. We adopted the Maxwell relationship $\epsilon_\infty \simeq n^2$ and calculated ϵ_∞ from the refractive index n. The determined solvation times τ_s are comparable to, but in any case not shorter than, the longitudinal relaxation times τ_L of the alcohols.
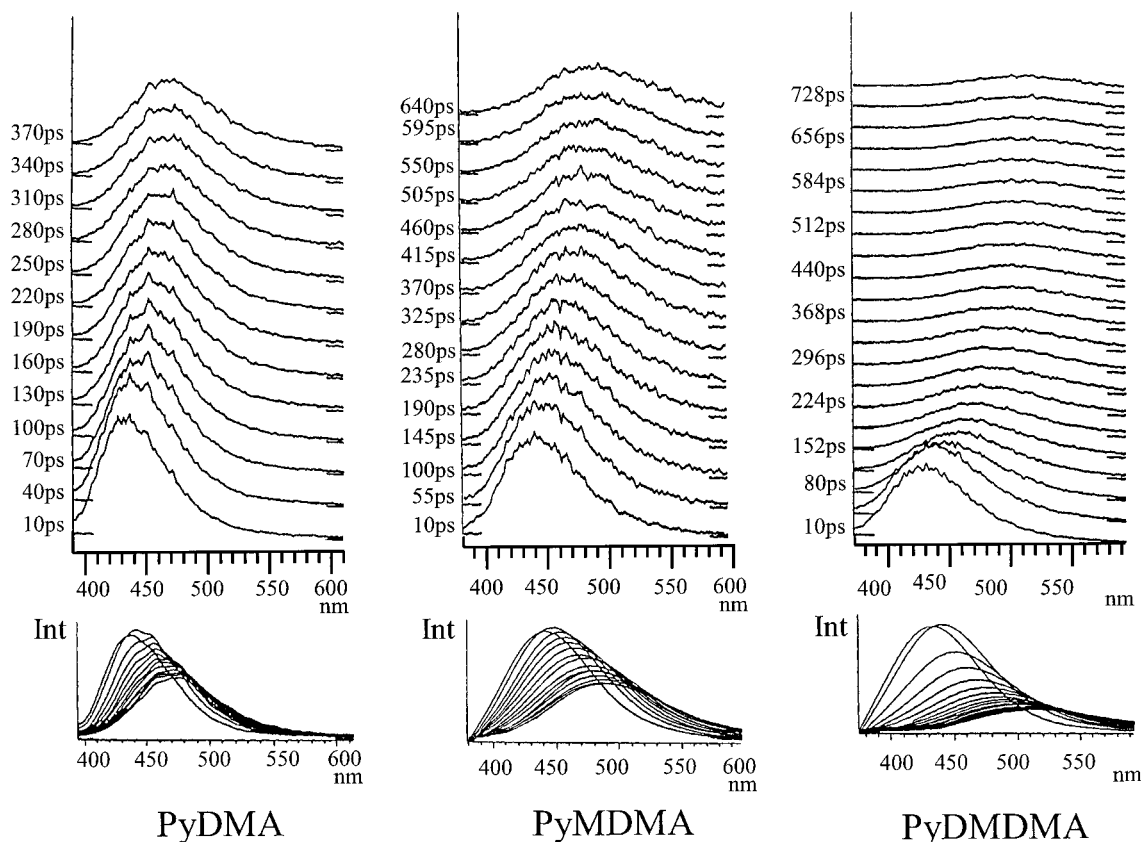
Figure 4. Time evolution of the CT fluorescence emission of PyDMA (left), PyMDMA (middle), and PyDMDMA (right) in hexanol. The streak images containing the intensity/wavelength/time information are displayed in binning mode.

TABLE 1: Observed Solvation Times Derived from the Time Dependent Stokes Shift of the CT Fluorescence Band of PyDMA, PyMDMA, and PyDMDMA (eqs 1–4)

substance	solvent	T/K	A_1/cm^{-1}	τ_1/ps	A_2/cm^{-1}	τ_2/ps	$\tilde{\nu}_\infty/ps$	τ_s^a/ps	τ_L/ps	τ_s/τ_L	τ_{LD}/ps	τ_s/τ_{LD}
PyDMA	hexOH	253	1953	1850	545	192	20403	1488	1130	1.32	1376	1.08
		273	1935	552	392	44	20626	466	429	1.09	535	0.87
		293	2029	227			20650	227	187	1.21	225	1.01
		296	1710	207			20780	207	161	1.29		
		313	1681	129			20770	129	95	1.35	113	1.14
	octOH	273	1657	1402	714	177	20800	1033	$\simeq 800$	1.29		
		293	1518	535	569	107	20935	418	353	1.18	418	1.00
		313	1534	241	365	45	21022	203	157	1.29	184	1.10
		333	1259	133	350	27	21150	110	89	1.35		
PyMDMA	hexOH	273	2224	605			19787	605	429	1.41	535	1.13
		293	1571	285			19884	285	187	1.52	225	1.27
		296	1289	274			19911	274	161	1.76		
	octOH	273	2034	1218			20003	1218	$\simeq 800$	1.56		
		293	1504	557			20218	557	353	1.58	418	1.33
PyDMDMA	hexOH	253	4271	1449	329	65	18703	1350	1130	1.19	1376	0.98
		273	4372	315			18788	593	429	1.38	535	1.11
		293	4266	255			18815	255	187	1.36	225	1.13
		296	4138	228			19080	228	161	1.42		
		313	3895	141			19267	141	95	1.48	113	1.25
	octOH	273	4062	1193			19094	1193	$\simeq 800$	1.49		
		293	3870	547			19247	510	353	1.44	418	1.22
		313	3597	245			19543	245	157	1.56	184	1.33
		333	2702	149			19785	149	89	1.67		
AnDMA	hexOH	293	2397[b]	333[b]			19320[b]	333[b]	187[b]	1.78[b]	225	1.48

^{a} ±10%. ^{b} From ref 2.

In model 2, the dipole character of the solvated chromophores is taken into account. Here, the interaction of a point dipole in a dielectric sphere with the dielectric constant ϵ_c is included leading to the relaxation time[27–29]

$$\tau_{LD} = \frac{2\epsilon_\infty + \epsilon_c}{2\epsilon + \epsilon_c}\tau_D \qquad (4)$$

For the sake of simplicity ϵ_c is set to unity. τ_{LD} values calculated with eq 4 are systematically 20% larger than τ_L relaxation times.

Independently, if τ_L or τ_{LD} is used, with increasing number of substituents the solvation times pass through a flat maximum for PyMDMA (see Table 1). As reported in reference 3, neither the stationary absorption (or emission) spectra nor the fluorescence lifetime measurements follow such dependences as shown

Directly Linked Donor−Acceptor System Dynamics

J. Phys. Chem. B, Vol. 105, No. 31, 2001 **7583**

TABLE 2: Fluorescence Intensity Decrease of PyDMDMA Calculated from the Data of Figure 4 and Adjusted for the Overlap with the Time Dependent Stokes Shift of the CT Band[a]

substance	solvent	T/K	B_1/a. u. (%)	τ'_1/ps	ϕ'_1/a. u.	B_2/a. u. (%)	τ'_2/ps	ϕ'_2/a. u.
PyDMDMA	hexOH	253	6491(64.8)	700	0.060	3529(35.2)	18400	0.940
		273	5773(57.5)	305	0.020	4260(42.5)	19300	0.980
		293	6128(53.8)	162	0.009	5257(46.2)	20200	0.991
		313	6031(53.3)	102	0.006	5285(46.7)	20800	0.994
	octOH	273	6708(65.7)	721	0.064	3509(34.3)	17700	0.936
		293	5909(57.1)	341	0.023	4303(42.1)	19600	0.977
		313	6069(51.4)	173	0.009	5736(48.6)	22100	0.991
		333	4868(41.1)	112	0.004	6963(58.9)	25000	0.996

[a] B_i are the exponential prefactors and τ'_1 the time constants (1/e) of the fluorescence decay components. $\phi'_i = B_i\tau'_1/\sum_i B_i\tau'_1$ are the relative fluorescence quantum yields. The monoexponential fluorescence decay times of PyDMA at 293 K are 3.7 ns (in hexOH), of PyMDMA 8.3 ns (in hexOH), and 7.6 ns (in octOH) ref 4.
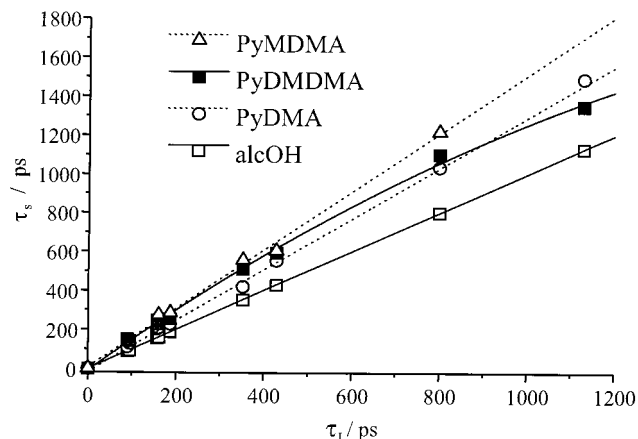
Figure 5. Comparison of the effective solvation relaxation time τ_s for PyDMA, PyMDMA, and PyDMDMA with the longitudinal relaxation time τ_L for hexOH and octOH (line with slope 1; see Table 1).

in Table 1. In these measurements, the order determined by structural changes is always PyDMA−PyMDMA−PyDMDMA. Taking the $n^3\tilde{\nu}^3$ correction into account, in the case of PyMDMA the wavelength corrected lifetime per volume, κ, decreases with increasing solvent polarity.[30] The κ values of PyDMA and PyDMDMA are solvent-independent within the error of experiment.

Figure 5 summarizes the different solvation kinetics by plotting the (averaged, cf. eq 2) solvation time, τ_s, against the longitudinal relaxation time, τ_L, of the solvent. The slope of the plots is not equal to unity. The plot shows not only show the reversed order in the dynamics, PyDMA−PyMDMA−PyDMDMA, but also a nonlinear dependence of τ_s on τ_L in the case of PyDMDMA. The deviation of the observed slower solvation times τ_s from τ_L, which is also expressed in the ratio τ_s/τ_L in Table 1, may be interpreted as additional intramolecular reorganizations that contribute as energy stabilization terms (in addition to the solvation) to the dynamic red shift of the fluorescence.

The same dependence is found by applying the improved model 2: if τ_L is plotted vs. τ_{LD} (not shown in this work) or if one compares the ratio τ_s/τ_{LD} in Table 1 with the ratio τ_s/τ_L, the former are, in general, closer to unity. However, in particular for PyDMDMA, the same systematic deviations or nonlinear dependencies are found as in the case of the ratio τ_s/τ_L.

In a first approximation, linear alcohols can be described as Debye continua. Experiments give evidence for nonlinear solvation dynamics with three different dispersion regions characterized by three different relaxation times τ_{D1}, τ_{D2}, and τ_{D3}.[25,26,31] Taking the three different dispersion regions into consideration, different τ_L and τ_{LD} times might be fitted in analogy to eqs 3 and 4. However, as can be seen from Table 1,

the kinetics of the CT solvation of PyDMA, PyMDMA, and PyDMDMA are mainly found to decay monoexponentially within the accuracy of the apparatus. Only the CT solvation times for PyDMA in octOH could be fitted biexponentially. And even these fitted times τ_1 and τ_2 do not sufficiently coincide with the relaxation times as measured by Garg and Smyth[26] (e.g., CT solvation relaxation times of PyDMA in octOH at $T = 313$ K: $\tau_1 = 241$ ps and $\tau_2 = 45$ ps, in comparison to the Debye relaxation times of octOH according to ref 26: $\tau_{D1} = 1780$ ps, $\tau_{D2} = 39$ ps, and $\tau_{D3} = 3.2$ ps), with exception of the (accidentally coinciding) "second" relaxation times τ_2 and τ_{D2}.

In addition to the (anomalous) solvation dynamics, PyDMDMA shows a biphasic intensity decay in contrast to PyDMA and PyMDMA, where the intensity decay could be fitted to a single-exponential function. Table 2 summarizes the data for PyDMDMA determined by spectro-streak and single photon counting measurements. The fit parameters B_1, B_2, and τ'_1 (the fast component to the biphasic decay function $B_1\exp(-t/\tau'_1) + B_2\exp(-t/\tau'_2)$) have been optimized applying the least-squares method while holding τ'_2 (the slow component) fixed. The nanosecond decay time τ'_2 could be measured separately with high precision ($\pm2\%$) since the τ'_1 times are shorter by a factor of at least 30. The striking similarity of the τ'_2 times and the solvation times τ_s possibly point at coupled processes during the stabilization dynamics of PyDMDMA.

As shown in the Figure 6, the temperature dependences of τ_s, τ_L, and τ'_1 according to $\ln(1/\tau_s, 1/\tau_L, \tau'_1) = k_i \exp(-E_a/RT)$ are comparable. In Figure 6, top, an Arrhenius plot is given for the solvation time τ_s. All three components show a slight deviation from a linear T^{-1} relation, though it is most pronounced in the case of PyDMDMA. The activation energies for the solvation processes are in the range of $(21-28)$ kJ mol^{-1}. Figure 6, bottom, summarizes the temperature dependences of the fast and slow fluorescence intensity decrease for PyDMDMA in hexOH and in octOH. Here, $\ln(1/\tau'_1)$ and $\ln(1/\tau'_2)$ of Table 2 are plotted against T^{-1} for comparison. The orders of magnitude of the slopes are comparable to that of Figure 6, top.

Transient Absorption Experiments. The transient absorption (TRABS) spectra of PyDMA and PyDMDMA in hexanol are shown in Figure 7. These spectra are corrected by subtraction of spontaneous fluorescence. Characteristic for the transient spectra of PyDMA are the negative changes in optical density that are caused by amplified stimulated emission (ASE) of the measuring background light. Due to solvent relaxation after CT generation, the system stabilizes and the gain spectrum shifts with time to the wavelength of the stationary limit in the red. The transient spectra of PyDMA are dominated by the characteristics of this compound as a potential "CT laser dye" with four-level properties and therefore low threshold.[2] Since the background amplification strongly influences the transient
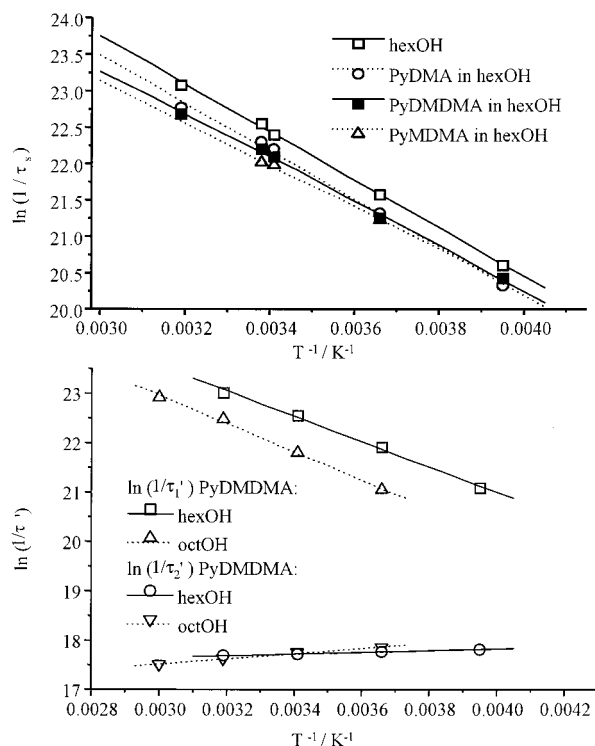
Figure 6. Top: Arrhenius plot of the temperature-dependent solvation response of PyDMA, PyMDMA, and PyDMDMA in hexanol. Bottom: Temperature dependence of fluorescence decay times τ'_1 and τ'_2 of PyDMDMA in hexOH (cf. Table 2).
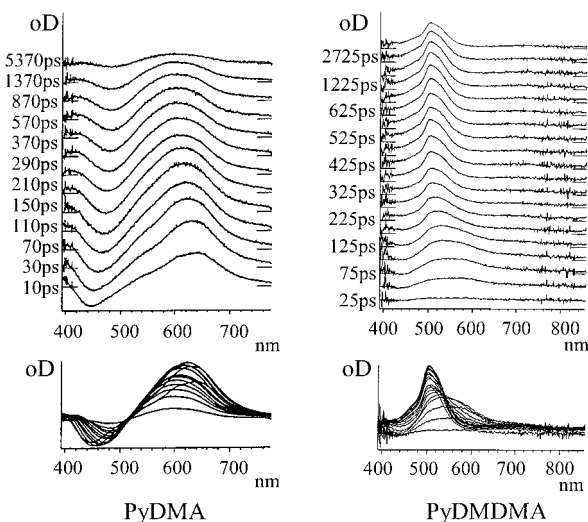
Figure 7. Transient absorption (TRABS) and gain spectra, respectively, of PyDMA (left) and PyDMDMA (right) in hexanol. The TRABS spectra of PyDMA are governed by the gain spectra. For PyDMDMA, the narrowing of the TRABS band points to a conformational change from an initial exciplex type species to a more radical ion-like species at later (> 500 ps) times. The influence of the gain spectrum in this case is small.

spectra and overlaps with the transient absorption band, a fit of the spectra at a time directly after light excitation and several hundred picoseconds later was not possible.

In PyDMDMA, at early times ASE also arises but much less pronounced than in the case of PyDMA. Therefore, the transient spectra reflect, like the fluorescence quantum yield measurements,[3] the minor laser efficiency of PyDMDMA compared to the more strongly lasing PyDMA. Since the stationary emission maximum of PyDMDMA in hexOH is located near 515 nm

(Figure 1), at times $t > 300$ ps the spectral range between 500 and 700 nm is characterized by a broad absorption band (which is typical for the CT exciplex species at early times) and a gradually sharpened band in the wavelength range of the acceptor radical anion moiety.[32] This characteristic distinction has been observed and discussed decades ago and is generally accepted since.[32] The gain contribution in the transient absorption spectra of PyDMDMA is minimal, particularly in the long time range (> 500 ps). These important features shall be considered in the discussion of a model that describes the reaction mechanism of PyDMDMA in protic solvents.

The TRABS apparatus also permits the registration of triplet spectra. In none of the systems studied was absorption of a ^{3}Py*-like species detected within the sensitivity of the apparatus.

Discussion of Mechanisms. The observed bathochromic shifts of the emission spectra as a consequence of a large excited-state dipole moment give evidence that the emitting state has pronounced CT character. No complications arise in the discussion of PyDMA and PyMDMA, whereas the kinetics of PyDMDMA show higher complexity as discussed in the following. First, one has to consider three characteristic time windows: (1) fast processes as ET (internal conversion) and vibrational relaxation in the subpicosecond range; not directly accessible in our experiments; (2) intermediate transient processes as solvation and concomitant intramolecular reorganizations on the time-scale of 100−300 ps; (3) fluorescence decay of nanosecond duration from a relaxed CT state.

For the spectro-streak and transient absorption measurements, PyDMA to PyDMDMA were excited with picosecond light pulses of 351 and 355 nm, respectively. These excitation wavelengths are in the spectral overlap region of the vibrationally highly excited $S_1^n \leftarrow S_0$ transition and the $S_2^0 \leftarrow S_0$ transition (see Figure 2). Note, that for the correct data treatment of measured spectroscopic features the adiabatic representation should be applied.[33] Also, quantum chemical calculations (ab initio or semiempirical) follow the adiabatic representation, since here the potential energy matrix is diagonal and not the nuclear kinetic energy matrix as in the diabatic representation. If one aims at comparing experimental results and theoretical calculations based on ab initio methods, it is therefore useful to work in the adiabatic representation. For a detailed discussion concerning these points, see ref 3. As a further consequence, in a *diabatic* picture the spectral overlap region of the S_1 and the S_2 state would correspond to the LE/CT overlap region. However, in an *adiabatic* representation this 1:1 correspondence is not valid anymore (see also ref 3). In the following we will concentrate on the *adiabatic* representation of ET and relaxation dynamics as it was defined in ref 3. Further complexity arises by the nonnegligible mixing of the S_2 state with the S_3 state, which is also pointed out in refs 3 and 34.

After the excitation in the S_1/S_2 overlap region, the relaxation of the system to the vibrationally relaxed CT state coincides with solvation or, in other words, concomitant intramolecular reorganization takes place in parallel with fluorescence, first from the CT state and followed by the fluorescence from the gradually solvated CT_s state. These processes take place on a 100−300 ps time-scale.

In the following, the extent of the adiabaticity of the ET (expressed in the adiabaticity parameter) is investigated. Since PyDMA to PyDMDMA are coupled ICT systems with strongly modulated photophysical characteristics due to the dominant vibronic coupling of the pyrene moiety, a clear separation of the photophysical reaction coordinate in a diabatic *inter*molecular (solvation) coordinate and a diabatic *intra*molecular

Directly Linked Donor−Acceptor System Dynamics

J. Phys. Chem. B, Vol. 105, No. 31, 2001 **7585**

reorganization coordinate cannot easily be made. The formalisms for perturbative treatments are also based on weakly interacting PESs,[35] which, however, is not the case particularly for the reported systems. The adiabaticity of an ET reaction can be quantified by the adiabaticity parameter[17,36]

$$\zeta = \frac{8\pi W^2 \tau_L}{\hbar N_a k_s} \qquad (5)$$

where W denotes the electronic coupling matrix element, N_a is Avogadro's constant, k_s is the solvent force constant, and τ_L is the longitudinal dielectric relaxation time. According to Rips et al.,[36] the solvent-controlled ET regime is realized when $\zeta \gg 1$. In previous work,[3] the coupling matrix element for PyDMA was determined to $W = 1.09$ kcal mol^{-1}. Assuming the same solvent properties as in the work of Tominaga et al.[17] ($k_s = 20$ kcal mol^{-1}, $\tau_L = 1$ ps; note that eq 5 is not given in atomic units), ζ is calculated to be 90, which is in the same order of magnitude as for AnDMA, which was $\zeta \simeq 80 \gg 1$. Therefore, it can be concluded that both systems are governed by strong adiabatic couplings and that PyDMA is even more strongly coupled than AnDMA (which is supported, e.g., by the difference in the absorption spectra).

However, in longer-chained alcohols, such as hexOH, τ_L increases to $\tau_L = 187$ ps. With an estimated solvent force constant of $k_s \simeq 15$ kcal mol^{-1} for PyDMA, ζ dramatically increases to $\zeta \simeq 2.4 \times 10^3 \gg 1$, meaning an even more solvent-controlled adiabatic ET reaction. For octOH, $\tau_L = 353$ ps leads to $\zeta \simeq 4.2 \times 10^3$. With respect to τ_L in Table 1, it can therefore be concluded that the larger τ_L (which in alcohols corresponds to an increase of the length of the carbon chain and a decrease of the dielectric properties of the solvent), the less the transiently formed CT dipole is stabilized and the more the ET is solvent-controlled (if it can be treated adiabatically).

If PyDMA, PyMDMA, PyDMDMA, (and AnDMA) in the same solvent hexOH are compared, the adiabaticity of the reaction and the solvent-assistance of the very fast ET are differently pronounced and reflected in the change of τ_s and τ_s/τ_L of Table 1 and Figure 5. At $T = 293$ K, one finds for PyDMA $\tau_s = 227$ ps and $\tau_s/\tau_L = 1.21$, which increases for PyMDMA to $\tau_s = 285$ ps and $\tau_s/\tau_L = 1.52$ and decreases for PyDMDMA to $\tau_s = 255$ ps and $\tau_s/\tau_L = 1.36$. AnDMA shows the slowest solvation relaxation behavior with $\tau_s = 333$ ps and $\tau_s/\tau_L = 1.78$.

As reported in ref 3, the coupling matrix element W marginally decreases in the opposite direction from W(PyDMA) $= 1.09$ kcal mol^{-1} to W(PyDMDMA) $= 0.9$ kcal mol^{-1}. Obviously, PyDMA shows the strongest coupling, resulting in an ultrafast ET reaction without pronounced intramolecular reorganization steps; the ET takes place nearly without any friction or reaction barrier. This fact is also reflected in the spectro-streak measurements where the refined τ_s is similar to the known τ_L. In previous work,[3] the ET step was estimated to occur on the time scale of 15 fs. However, the experimental verification of this value has still to be given. Even if the coupling is still considerable, the smaller coupling constant in AnDMA ($W = 0.8$ kcal mol^{-1}) leads to a slightly slower ET decay time < 150 fs[17] and intramolecular reorganization might play a somewhat more important role for the ET reaction than in the case of PyDMA. This would result in a larger discrepancy of τ_s compared to τ_L.

For the same reason, one could expect that τ_s/τ_L increases from PyDMA to PyDMDMA. The increase is found for PyMDMA; however, for PyDMDMA the ratio again decreases
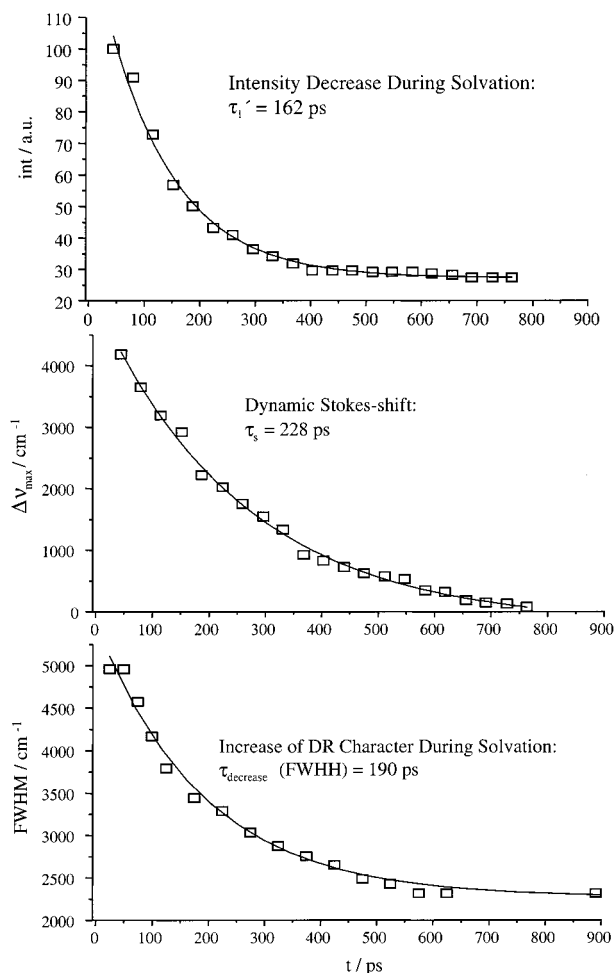

Figure 8. Comparison of the fast component of the fluorescence intensity decay time τ'_1 (top), the solvation relaxation time τ_s (middle), and the time course of the fwhm change of the transient spectra $\tau_{decrease}$ (fwhm) (bottom) of PyDMDMA in hexOH (DR = diradical). Top and middle are results from the numerical treatment of the spectro-streak measurements, bottom is a result of the numerical treatment of the transient spectra.

as seen in Table 1, in Figure 5 and in Figure 6. To understand this anomalous solvation behavior of PyDMDMA, the decay time of the ICT fluorescence $\tau'_1 = 162$ ps ($T = 293$ K, Table 2) and the relaxation time of the ICT solvation $\tau_s = 228$ ps ($T = 293$ K, Table 1) are plotted in Figure 8 and compared with the numerical treatment of the transient spectra in Figure 7. Since the gradual sharpening of the transient band of PyDMDMA in the wavelength range of the acceptor radical anion[32] can be assigned to a species with diradical character, the fwhm of this transient band is a measure of the dynamic transition from a ICT state to the diradical (DR) state. Figure 8, bottom, shows the decay behavior from the broad band with fwhm = 5000 cm^{-1} to the narrow band with fwhm = 2500 cm^{-1} with a transition time of $\tau_{decrease} = 190$ ps. All three decay times, τ'_1, τ_s, and $\tau_{decrease}$, are (within about ±18%) of the same order of magnitude.

This fact, in conjunction with other observations, e.g., the decrease of the absolute CT fluorescence quantum yield of $\Phi_F = 0.65$ (PyDMDMA in hexOH) compared to $\Phi_F = 0.97$ (PyDMA in hexOH), might be rationalized by the introduction of a third nonfluorescing state in the reaction scheme of PyDMDMA, providing a nonradiative deactivation channel. Figure 9 depicts an adiabatic mechanism suggesting a solvent-driven transition from a fluorescing ICT species to a nonfluo-
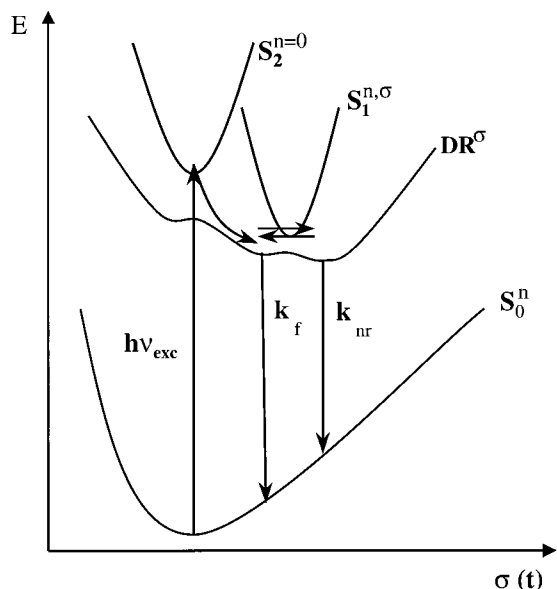
Figure 9. Adiabatic reaction scheme for the deactivation of Py-DMDMA. The arrow indicates the solvation process as a function of time ($\sigma(t)$) as manifested by the observed large bathochromic Stokes shift. The solvent-supported fluorescence quenching is expressed in an adiabatic transition to a species with diradical (DR) character.

rescing species with diradical character for PyDMDMA. In the course of the described solvation process σ, fluorescence emission properties, represented by the solvation dependent fluorescence rate coefficient, k_f, gradually decrease until the fully solvated and relaxed species S_1^σ (fluorescing) and DR^σ (non-fluorescing) are reached.

The experimental finding that the degree of solvation was observed to be less pronounced with increasing solvent polarity (from *n*-hexane to acetonitrile) compared to systems where the separation of A^- and D^+ moieties is possible[3] also supports the idea of a coupling between the solvation process and the CT emission probability in the case of the pre-twisted Py-DMDMA. This is typical for closely linked A/D systems where solvent-shared $A^- D^+$ pairs hardly do exist: solvent molecules with large dipole moments (high permittivity in the bulk, e.g., acetonitrile) cannot separate the linked moieties and therefore decrease the Coulomb energy much less.

IV. Conclusions

In this work kinetic studies of the fast dynamic Stokes shift of hexOH and octOH around optically generated CT dipoles have been presented. Three covalently linked electron donor–acceptor systems of the type pyrene (acceptor)/dimethylaniline (donor) varying in methyl substitution on the donor part (PyDMA, PyMDMA, and PyDMDMA) were used as model CT compounds. The CT species were optically generated by UV absorption. The fast spectroscopic changes related to solvents and solvent responses were observed by the picosecond spectro-streak technique (351 nm excitation wavelength) and picosecond transient absorption spectroscopy (355 nm excitation wavelength).

In PyDMA, PyMDMA, and PyDMDMA, the kinetic treatment of the dynamic Stokes shift detected by the spectro-streak photometer leads to solvation relaxation times of hexOH and octOH comparable with, but 10% larger than the longitudinal dielectric relaxation times of the neat alcohols. The deviation increases from PyDMA to PyMDMA and decreases in the case of PyDMDMA. Only in the case of PyDMDMA does the intensity analysis of the spectro-streak measurements in time

yield a biphasic fluorescence decay with a fast component on a time scale comparable to the solvation relaxation times and comparable to the change of the fwhm of the transient absorption band.

Characteristic for all three compounds is the high fluorescence quantum yield. Furthermore, the gain spectrum (generated by amplification of the measuring background light) influences the transient absorption spectrum in the wavelength range of the CT emission band, strongly in PyDMA and to a minor extent in PyDMDMA. Therefore, the time evolution of the transient emission and absorption spectra mainly reflects both the dynamics of the solvent stabilization around the CT dipole and the deactivation of the CT state.

Another important piece of information is derived from the transient absorption at times > 300 ps. The relatively narrow absorption band of PyDMDMA (in the wavelength range of the pyrene anion spectrum near 500 nm) indicates the generation of a transient species with diradical character. It is concluded that this DR species exhibits a reduced emission probability that is due to a solvation (σ)-dependent change of the electronic structure (cf. $k_f/n^3\tilde\nu^3$). Gould and Farid[37] have recently critically examined the relationship between CT fluorescence from a contact radical ion pair and a nonradiative (thermal) ET in bimolecular donor–acceptor systems. It is planned to apply their approach to elucidate the nature of the DR state of PyDMDMA as conjectured from the present experimental data.

A further possibility of direct experimental determination of the structural rearrangements of CT compounds in time could be time-resolved X-ray diffraction based on a pulsed (UV light) pump (X-rays) probe technique with a synchrotron source. Work in this field is in progress at the European Synchrotron Radiation Facility (ESRF) at Grenoble, France.[38–40]

References and Notes

(1) Dapprich, J.; Walter, N.; Salinque, F.; Staerk, H. *J. Fluoresc.* **1997**, *7*, 87 S.

(2) Wiessner, A.; Hüttmann, G.; Kühnle, W.; Staerk, H. *J. Phys. Chem.* **1995**, *99*, 14923.

(3) Techert, S.; Schmatz, S.; Wiessner, A.; Staerk, H. *J. Phys. Chem. A* **2000**, *104*, 5700.

(4) Soujanya, T.; Philippon, A.; Leroy, S.; Vallier, M.; Fages, F. *J. Phys. Chem. A* **2000**, *104*, 9408.

(5) Simon, J. A.; Curry, S. L.; Schmehl, R. H.; Schatz, T. R.; Piotrowiak, P.; Jin, X.; Thummel, R. P. *J. Am. Chem. Soc.* **1997**, *119*, 11012.

(6) Weller, A., unpublished results.

(7) Techert, S.; Schotte, F.; Wulff, M. *Phys. Rev. Lett.* **2001**, *86*(10), 2030.

(8) Techert, S.; Schotte, F.; Wulff, M. *Highlights ESRF* **2001**, *5*, 14.

(9) Hagopian, S.; Singer, A. *J. Am. Chem. Soc.* **1985**, *107*, 1874.

(10) Tseng, J. C.-C.; Singer, A. *J. Phys. Chem.* **1989**, *93*, 7092.

(11) Bree, A.; Vilkos, V. V. B. *Spectrochim. Acta* **1972**, *27 A*, 2333.

(12) Klimova, L. A. *Chem. Phys. Lett.* **1970**, *4*, 537.

(13) Bree, A.; Vilkos, V. V. B. *Opt. Spectrosc.* **1963**, *14*, 185.

(14) Onkelinx, A.; Schweitzer, G.; De Schryver, F. C.; Miyasaka, H.; der Auweraer, M. V.; Asahi, T.; Masahura, H.; Fukumura, H.; Yashima, A.; Iwai, K. *J. Phys. Chem. A* **1997**, *A 101*, 5054.

(15) Okada, T.; Mataga, N.; Baumann, W.; Siemarczuk, A. *J. Phys. Chem.* **1987**, *91*, 4490.

(16) Tominaga, K.; Walker, G. C.; Jarzeba, W.; Barbara, P. F. *J. Phys. Chem.* **1991**, *95*, 10475.

(17) Tominaga, K.; Walker, G. C.; Kang, T. J.; Barbara, P. F.; Fonseca, T. *J. Phys. Chem.* **1991**, *95*, 10475.

(18) Dey, J.; Warner, I. M. *J. Phys. Chem.* **1997**, *A101*, 4872.

(19) Herbich, J.; Kapturkievicz, A. *Chem. Phys.* **1993**, *158*, 143.

Directly Linked Donor−Acceptor System Dynamics

J. Phys. Chem. B, Vol. 105, No. 31, 2001 **7587**

(20) Wiessner, A.; Staerk, H. *Rev. Sci. Instrum.* **1993**, *64*, 3430.

(21) Wiessner, A. Ph.D. Thesis; Georg-August-Universität: Göttingen, 1994.

(22) Hüttmann, G. Ph.D. Thesis; Georg-August-Universität: Göttingen, 1992.

(23) Hüttmann, G.; Kühnle, W.; Staerk, H. *J. Photochem. Photobiol.* **1993**, *A 70*, 83.

(24) Maroncelli, M.; Fleming, G. R. *J. Chem. Phys.* **1987**, *86*, 6221.

(25) Fröhlich, H. *Theory of Dielectrics*; Oxford Clarendon Press: Oxford, 1949.

(26) Garg, S. K.; Smyth, C. P. *J. Phys. Chem.* **1965**, *69*, 1294.

(27) Bagchi, B.; Oxtoby, D. W.; Fleming, G. W. *Chem. Phys.* **1984**, *86*, 257.

(28) der Zwan, G. V.; Hynes, J. T. *J. Phys. Chem.* **1985**, *89*, 4181.

(29) Chandra, A.; Bagchi, B. *Chem. Phys. Lett.* **1988**, *47*, 151.

(30) $\kappa = \kappa_{CT}/\langle n^3 \tilde{v}^3 \rangle$, where $\kappa_{CT} = \Phi_{CT}/\tau_{CT}$ and $\langle n^3 \tilde{v}^3 \rangle$ is a band averaged correction factor; for details see ref 3.

(31) Barthel, J.; Bachhuber, K.; Buchner, R.; Hetzenauer, H. *Chem. Phys. Lett.* **1990**, *165*, 369.

(32) Potashnik, R.; Goldschmidt, C. R.; Ottolenghi, M.; Weller, A. *J. Chem. Phys.* **1971**, *55*, 5344.

(33) Herzberg, G. *Molecular Spectra and Molecular Structure, III. Electronic Spectra and Electronic Structure of Polyatomic Molecules*; Robert E. Krieger Publishing Company: Malabar, Florida, 1991.

(34) Herbich, J.; Kapturkiewicz, A. *J. Am. Chem. Soc.* **1998**, *120*, 1014.

(35) Sumi, H.; Marcus, R. A. *J. Chem. Phys.* **1985**, *84*, 4894.

(36) Rips, I.; Klafter, J.; Jortner, J. *J. Phys. Chem.* **1990**, *94*, 8557.

(37) Gould, I. R.; Farid, S. *J. Photochem. Photobiol.* **1992**, *A-65*, 133.

(38) Techert, S.; Wulff, M., in preparation.

(39) Schotte, F.; Techert, S.; Anfinrud, P. A.; Srajer, V.; Moffat, K.; Wulff, M. In *Handbook of Synchrotron Radiation 5*; Mills, D., Ed.; John Wiley & Sons: New York, 2000.

(40) Techert, S.; Schmatz, S. *Z. Phys. Chem.* **2001**, in press.